PERGAMON

International Journal of Heat and Mass Transfer 43 (2000) 1409–1424

International Journal of HEAT and MASS TRANSFER

www.elsevier.com/locate/ijhmt

Transient, three-dimensional heat transfer model for the laser assisted machining of silicon nitride: I. Comparison of predictions with measured surface temperature histories

Jay C. Rozzi[a,*], Frank E. Pfefferkorn[a], Frank P. Incropera[b], Yung C. Shin[a]

[a] *Laser Assisted Materials Processing Laboratory, School of Mechanical Engineering, Purdue University, USA*
[b] *Aerospace and Mechanical Engineering Department, University of Notre Dame, USA*

Received 5 August 1998; received in revised form 25 June 1999

Abstract

Laser assisted machining (LAM), in which the material is locally heated by an intense laser source prior to material removal, provides an alternative machining process with the potential to yield higher material removal rates, as well as improved control of workpiece properties and geometry, for difficult-to-machine materials such as structural ceramics. To assess the feasibility of the LAM process and to obtain an improved understanding of governing physical phenomena, experiments have been performed to determine the thermal response of a rotating silicon nitride workpiece undergoing heating by a translating CO_2 laser and material removal by a cutting tool. Using a focused laser pyrometer, surface temperature histories were measured to determine the effect of the rotational and translational speeds, the depth of cut, the laser-tool lead distance, and the laser beam diameter and power on thermal conditions. The measurements are in excellent agreement with predictions based on a transient, three-dimensional numerical solution of the heating and material removal processes. The temperature distribution within the unmachined workpiece is most strongly influenced by the laser power and laser-tool lead distance, as well as by the laser/tool translational velocity. A minimum allowable operating temperature in the material removal region corresponds to the YSiAlON glass transition temperature, below which tool fracture may occur. In a companion paper [1], the numerical model is used to further elucidate thermal conditions associated with laser assisted machining.

1. Introduction

Laser assisted machining (LAM) has recently been considered as an alternative process for machining ceramic materials. In LAM, the laser is used as an intense heat source to change the ceramic deformation behavior from brittle to ductile just prior to material removal, without melting or sublimation of the workpiece. Although the feasibility of LAM has been demonstrated [2], underlying physical mechanisms are not well understood and a comprehensive thermo-mechanical model of the heating and material removal processes has yet to be developed and validated through comparisons with experimental results. These deficiencies must be addressed if intelligent control

* Corresponding author. Creare, Inc., Etna Rd., P.O. Box, Hanover, NH 03755, USA. Tel.: +1-603-643-3800; fax: +1-603-643-4657.
E-mail address: jcr@creare.com (J.C. Rozzi).

0017-9310/00/$ - see front matter
PII: S0017-9310(99)00217-3

Nomenclature

A_{flank}	flank wear scar area (m^2)
c_p	specific heat at constant pressure (J/kg K)
d	depth of cut (m)
D	diameter (m)
E	emissive power (W/m^2)
$\dot{E}$	rate of energy generation or dissipation (W)
F	force (N)
f_ℓ	function describing the area of laser heating (dimensionless)
h	heat transfer coefficient (W/m^2 K)
H_j	jet nozzle-to-workpiece distance (m)
i	enthalpy (J/kg)
k	thermal conductivity (W/m K)
L_{cv}	length of computational domain (m)
L_f	tool feed in single point machining (m)
L_ℓ	laser-tool lead distance (m)
$L_{\ell,a}$	average distance between the laser center and the edge of the material removal plane (m)
$\dot{m}$	mass flow rate (kg/s)
$\dot{m}''$	mass flux (kg/s m^2)
N	total number of control volumes
Nu	Nusselt number
p	pressure (Pa)
P	power (W)
q''	heat flux (W/m^2)
q'''	volumetric heat generation (W/m^3)
r	radius (m)
$r_{\ell,p}$	radius of the beam plane representing 86.5% of the total beam power (m)
r_t	radius of the tool insert (m)
r_w	workpiece radius (m)
$r_{w,m}$	machined workpiece radius (m)
$R_{\text{flank,w}}$	fraction of frictional heat generated at the tool flank which is conducted into the workpiece for single point machining
Re	Reynolds number
s_{psz}	thickness of the primary shear zone (m)
t	time (s)
t_p	preheat time (s)
T	temperature (K)
$T_{s,ch}$	near-chamfer surface temperature (K)
$\overline{\Delta T}_w$	average temperature difference between the workpiece and the cutting tool flank (K)
$\forall$	volume of primary shear zone (m^3)
V_{chip}	average chip velocity (m/s)
V_w	workpiece velocity (m/s)
$\bar{V}_w$	average workplace velocity perpendicular to the cutting tool over the depth of cut (m/s)
V_z	laser or laser/tool translational velocity (m/s)
VB_{max}	maximum extent of flank wear region (m)
z	axial coordinate (m)
z_c	axial location of the laser center (m)
z_{fe}	axial location of the workpiece free end (m)
$z_{fe,o}$	initial axial location of the workpiece free end (m)
z_{ch}	axial location of chamfer (m)

Greek symbols

α_ℓ	absorptivity of the unmachined (sintered) workpiece surface to irradiation from the CO_2 laser
$\alpha_{\ell,m}$	absorptivity of the machined workpiece surface to irradiation from the CO_2 laser
ε	emissivity of the unmachined (sintered) workpiece surface; strain
ε_m	emissivity of the machined workpiece surface
$\dot{\varepsilon}$	strain rate (s^{-1})
ϕ	circumferential coordinate (rad)
ϕ_c	circumferential location of the laser center (rad)
ϕ_{flank}	circumferential extent of flank wear region for single point machining (rad)
ϕ_ℓ	circumferential distance between the laser center and the material removal plane (rad)
φ_ℓ	fraction of the energy of deformation dissipated as thermal energy
μ	coefficient of friction
ν	workpiece rotational speed (rpm)
ρ	density (kg/m^3)
σ	Stefan–Boltzmann constant (W/m^2 K^4), stress (N/m^2)
$\bar{\sigma}$	effective flow stress (N/m^2)
ω	workpiece rotational speed (rad/s)
Ω_ℓ	lead or clearance angle (rad)

Subscripts

a	average
abs	absorbed
c	cutting direction or source geometric center
ct	chip–tool interface
conv	convention
f	feed direction
flank	tool flank face
j	laser gas assist jet
ℓ	laser beam

m	machined surface	t	tool
max	maximum	sur	surroundings
mr	material removal plane	w	workpiece
pl	plastic deformation	worn	worn cutting tool
rad	radiation	r, ϕ, z	cylindrical coordinate directions
ref	reference condition	∞	ambient air
s	primary shear zone		

schemes capable of optimizing LAM processes are to be established.

Previous investigators [2–5] have conducted plasma and laser assisted machining of various advanced ceramic materials, including zirconia, alumina, and silicon nitride. The studies suffer from exiguous characterizations of experimental conditions and temperature measurement techniques and absence of a process model. For example, temperature measurements have been made for various ceramic models [3,4] but without specification of the measurement location and/or the measurement technique. In studies of laser assisted machining of silicon nitride using CO_2 (10.6 μm) and Nd:YAG (1.06 μm) lasers [2,5], it was found that a preheat phase, during which no laser/tool translational motion occurs relative to the rotating workpiece, was necessary to avoid cutting tool fracture upon initiation of material removal, and that less power was required to facilitate material removal using the Nd:YAG laser. Although the implication is that the silicon nitride surfaces were spectral, with more energy being absorbed at the lower wavelength, no mention was made of surface radiative properties.

For rotating silicon nitride workpieces heated by a translating CO_2 laser *without material removal*, surface temperatures were measured using a laser pyrometer and were compared with predictions based on a transient, three-dimensional model [6]. Good agreement was obtained between the measured and predicted surface temperature histories for a wide range of operating conditions. With increasing workpiece rotational speed, temperatures in proximity to the laser spot decreased, while those at circumferential locations further removed from the laser increased. Near-laser temperatures decreased with increasing beam diameter, while energy deposition by the laser and, correspondingly, workpiece surface temperatures increased with decreasing laser transitional speed and increasing laser power.

The present study represents the first attempt to develop and validate a comprehensive thermo-mechanical model for LAM. A transient, three-dimensional heat transfer model which embodies pertinent physical features of the heating and material removal processes has been constructed, and predictions have been compared to measurements of the surface temperature history for rotating cylindrical silicon nitride workpieces.

2. Model geometry

One option for constructing a physically realistic model of LAM entails fixing a nonrotating coordinate system to the free end of the workpiece, as was done for laser heating without machining [6]. As the laser moves away from the fixed origin of the coordinate system at a prescribed translational velocity, V_z, it is displaced a distance, $\Delta z = V_z \Delta t$, for each time step, Δt. To attain sufficient spatial resolution of the near-laser surface temperature distribution beneath a 3 mm diameter laser spot, 10–15 control volumes were required, with corresponding values of Δz ranging from 0.2 to 0.3 mm [6]. A representative heated length of 15 mm would then require from 50 to 75 control volumes in the axial direction. For laser assisted machining, however, the machining zone for a representative feed of 0.1 mm/rev, corresponding to workpiece rotational and laser/tool translational speeds of 1000 rpm and 100 mm/min, respectively, has an axial length of 0.1 mm. Adequate spatial resolution of the temperature distribution in this region would then require values of Δz approximately less than 0.025 mm, and for a machined length of 15 mm, at least 600 control volumes would be required in the axial direction.

To avoid the extensive computational times associated with a large number of z-direction control volumes, a formulation in which the coordinate system is fixed relative to the laser has been utilized (Fig. 1). The transient numerical calculation is divided into two phases. In phase I, no workpiece translational motion occurs relative to the laser source, and the free end of the workpiece is preheated before cutting is initiated. This phase is necessary [5] to avoid cutting tool fracture at the beginning of material removal. In phase II, material removal is initiated with simultaneous movement of the workpiece free end toward $z = 0$. Because the computational domain remains fixed with respect to the laser and cutting tool, control volumes can be more densely concentrated in regions of high temperature gradients and material removal, thereby increasing computational efficiency and accuracy.

Representation of the portion of the computational domain that does not involve thermal energy transport by conduction or advection, and whose initial length during the preheat phase, $z_{fe,o}$

(Fig. 1), corresponds to the desired machining length, was achieved by setting the thermal conductivity of the inactive control volumes to a very small (negligible) value. Using this procedure, trial calculations were performed without material removal, and excellent agreement was obtained with numerical predictions for equivalent physical conditions, but for which the coordinate system was fixed to the workpiece free end.

Following initiation of the material removal phase, the workpiece geometry corresponds to that illustrated in Fig. 2 for a cutting tool with zero radius ($r_t=0$). A helical chamfer, whose shape is defined by the cutting tool geometry and feed rate, represents the boundary between removed and unremoved material. On the chamfer, the small r–z plane at $\phi=0$ corresponds to the location of material removal and its position with respect to the laser geometric center is specified by ϕ_ℓ and L_ℓ. As viewed in the positive circumferential direction from $\phi=0$, the inset of Fig. 2 displays the material removal plane corresponding to the actual tool geometry. The lead angle, Ω_ℓ, is inclined toward the laser source, and L_ℓ is the distance between the laser geometric center and the most distant edge of the material removal plane. The width of the material removal plane away from the tool cutting edge is specified by the tool feed, L_f. From calculations performed for laser heating without machining, axial temperature gradients within the shaded area were found to be negligible for ϕ_ℓ, L_ℓ, and r_t values typical of LAM. The chamfer has therefore been approximated by a plane of zero lead angle ($\Omega_\ell=0$ deg) and equivalent area located at the average distance, $L_{\ell,a}$, between the laser center and the edge of the material removal plane (Fig. 2), which is given by,

$$L_{\ell,a} = L_\ell - (d/2)\tan(\Omega_\ell) - r_t\left[1-\sin(\Omega_\ell)\right]\left\{\left[\tan(\pi/4-\Omega_\ell/2)\right]^{-1}-\tan(\Omega_\ell)\right\} \quad (1)$$

It is possible that optimal laser assisted machining may be achieved by positioning the laser in such a way as to overlap the chamfer, resulting in some portion of the laser heating the machined workpiece surface. The

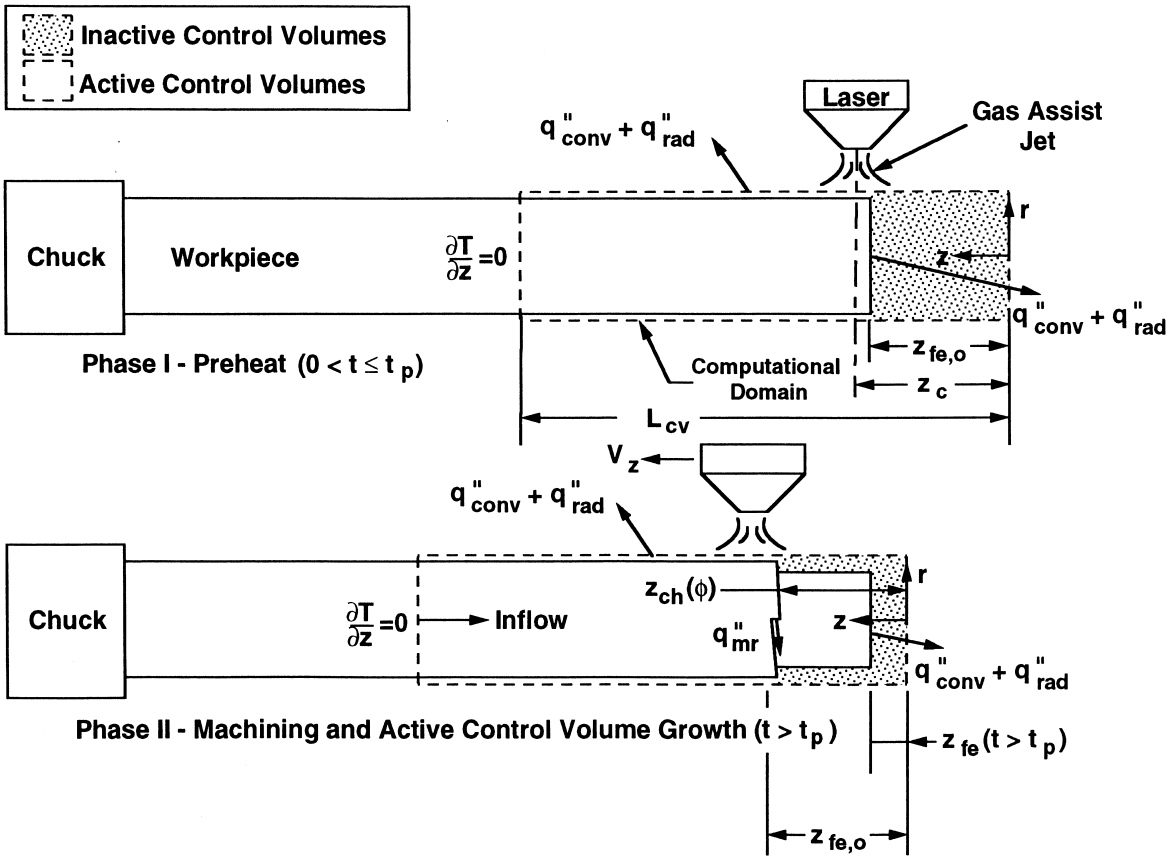

Fig. 1. Schematic of the model for the transient calculation of laser heating on a rotating workpiece with preheating and machining.

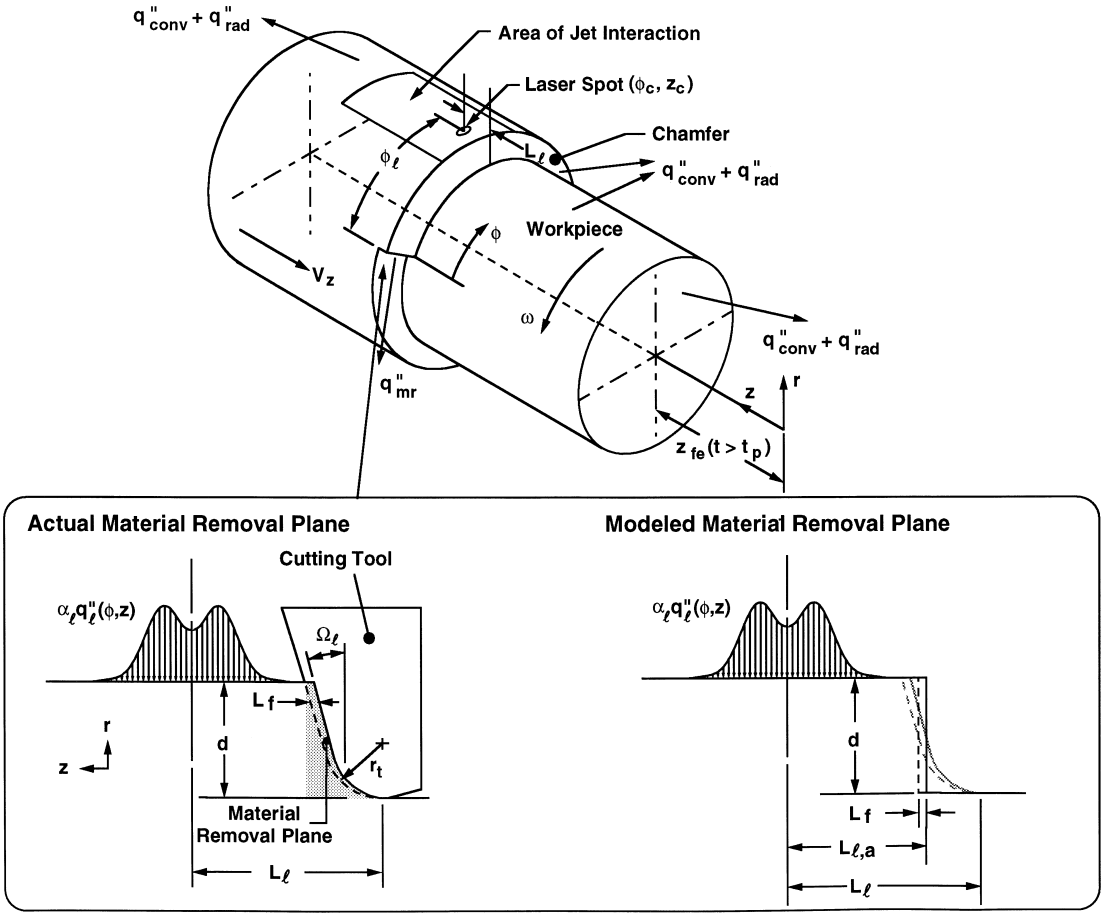

Fig. 2. Geometry of the laser assisted machining process.

portion of the laser flux incident on the chamfer itself is neglected, consistent with the assumption of zero lead angle.

Representation of phase II, during which mass inflow at $z = L_{cv}$ is exactly balanced by material removal and active control volume growth, is illustrated in Fig. 3 where q'''_{pl} and q'''_{flank} represent volumetric energy generation due to plastic work and a boundary heat flux arising from frictional (abrasive) wear between the workpiece and the cutting tool flank, respectively. The extent of the chamfer in the ϕ-direction was represented by a series of discrete steps, and heat transfer by radiation and convention from the chamfer and machined surface to the surroundings was considered.

3. Mathematical formulation and assumptions

The preheat phase of the numerical calculation corresponded to consideration of radial, axial, and circumferential conduction in a rotating cylinder with a stationary laser source. The governing heat equation and boundary conditions correspond to those given for laser heating without machining [6] with $V_z = 0$ and are not repeated.

At the initiation of material removal (phase II), the interface between removed and remaining materials is given by,

$$z_{ch}(\phi) = (z_c - L_{\ell,a}) + \frac{V_z}{\omega}\left[1 - \left(\frac{\phi}{2\pi}\right)\right] \quad (2)$$

where the material plane is placed at $\phi = 0$ deg and the lead angle and the tool radius have been neglected.

For transient heat transfer in a rotating cylinder and a nonrotating coordinate system attached to the translating laser and cutting tool, the governing heat equation may be expressed as,

$$\frac{1}{r}\frac{\partial}{\partial r}\left(kr\frac{\partial T}{\partial r}\right)+\frac{1}{r^2}\frac{\partial}{\partial \phi}\left(k\frac{\partial T}{\partial \phi}\right)+\frac{\partial}{\partial z}\left(k\frac{\partial T}{\partial z}\right)+q'''$$
$$=\rho c_p\omega\frac{\partial T}{\partial \phi}+\rho c_p V_z\frac{\partial T}{\partial z}+\rho c_p\frac{\partial T}{\partial t} \quad (3)$$

where the thermal conductivity has been assumed to be isotropic. The z-direction advection term arises due to attachment of the coordinate system relative to the laser and cutting tool, rather than to the workpiece free end. Because the laser beam diameter, D_ℓ, is small relative to the workpiece diameter, the function describing the area of laser heating may be approximated as,

$$f_\ell(r,z,\phi)=\sqrt{\left[r(\phi-\phi_c)\right]^2+(z-z_c)^2}/r_\ell\leqslant 1 \quad (4)$$

where $(\phi_c,\ z_c)$ and r specify the location of the laser geometric center and the radial location of laser heating for both the unmachined (r_w) and machined ($r_w=r_w-d$) workpiece surfaces. For the process times associated with LAM, irradiation from the surroundings will be negligible compared to surface emission. The radial boundary conditions on the unmachined workpiece surface therefore correspond to,

$$k\frac{\partial T}{\partial r}\bigg|_{r=r_w}=\alpha_\ell q''_\ell-q''_{conv}-E(T), \quad (5a)$$

for $z>z_{ch}(\phi)$ and $f_\ell(r,\ z,\ \phi)\leqslant 1$ on the laser spot, and

$$k\frac{\partial T}{\partial r}\bigg|_{r=r_w}=-q''_{conv}-E(T), \quad (5b)$$

for $z>z_{ch}(\phi)$ and $f_\ell(r,\ z,\ \phi)>1$, where $E=\varepsilon\sigma T^4$. On the machined surface, the radial boundary conditions are,

$$k\frac{\partial T}{\partial r}\bigg|_{r=r_{w,\,m}}=\alpha_{\ell,\,m}q''_\ell-q''_{conv}-E(T), \quad (5c)$$

for $z<z_{ch}(\phi)$ and $f_\ell(r,\ z,\ \phi)\leqslant 1$ on the laser spot when the laser overlaps the chamfer (Fig. 3) and spreading of the laser beam from $r=r_w$ to $r=r_w-d$ is negligible, and

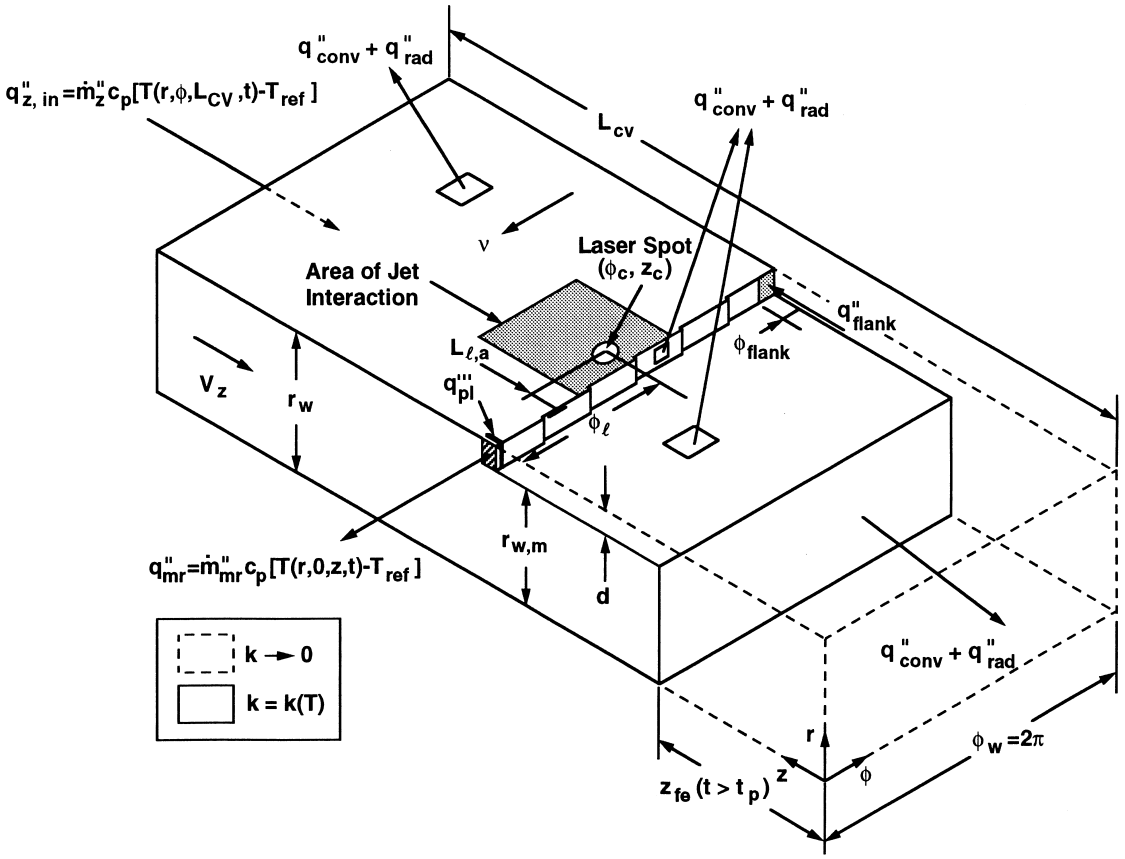

Fig. 3. Computational domain after the initiation of material removed.

$$k\frac{\partial T}{\partial r}\bigg|_{r=r_{w,\,m}} = -q''_{conv} - E(T), \tag{5d}$$

for $z < z_{ch}(\phi)$ and $f_\ell(r, z, \phi) > 1$. Although workpiece surface conditions are asymmetrical, asymmetries are attenuated with decreasing radius, and it is an excellent approximation to prescribe symmetry conditions at the workpiece centerline.

$$k\frac{\partial T}{\partial r}\bigg|_{r=0} = 0 \tag{5e}$$

On the interface between removed and remaining material, the following energy balance is applied,

$$k\frac{\partial T}{\partial z}\bigg|_{z=z_{ch}(\phi)} = q''_{conv} + E(T), \tag{6a}$$

for $r_{w,m} \leqslant r \leqslant r_w$ and $0 < \phi \leqslant 2\pi - \phi_{flank}$, and

$$k\frac{\partial T}{\partial z}\bigg|_{z=z_{ch}(\phi)} = -q''_{flank} \tag{6b}$$

for $r_{w,m} \leqslant r \leqslant r_w$ and $2\pi = \phi_{flank} < \phi \leqslant 2\pi$. Heating at the tool flank has been approximated in terms of a uniform heat flux, whose magnitude and spatial extent are obtained from experimental cutting force data. Since the chamfer is helical, the contribution of circumferential conduction at the chamfer surface has been neglected. At the end faces of the computational domain,

$$k\frac{\partial T}{\partial z}\bigg|_{\substack{z=z_{fe,o}(t\leqslant t_p)\\ z=z_{fe}(t>t_p)}} = q''_{conv} + E(T) \tag{6c}$$

where $z_{fe}(t > t_p) = z_{fe,o} - V_z(t - t_p)$ and $z_{fe,o}$ and t_p are the initial position of the workpiece free end and the preheat time, respectively. A zero heat flux condition is assumed at the inflow boundary,

$$\frac{\partial T}{\partial z}\bigg|_{z=L_{cv}} = 0. \tag{6d}$$

At the material removal plane, energy advection out of the system is represented by,

$$-\frac{k}{r}\frac{\partial T}{\partial \phi}\bigg|_{\phi=0} = \rho c_p r\omega(T - T_{ref}), \tag{7a}$$

for $r_{w,m} \leqslant r \leqslant r_w$. Away from the material removal location, circumferential boundary conditions correspond to continuity between temperatures and temperature gradients at ϕ and $\phi + 2\pi$. Hence,

$$T(r, \phi, z) = T(r, \phi + 2\pi, z) \tag{7b}$$

$$\frac{\partial T}{\partial \phi}\bigg|_{\phi} = \frac{\partial T}{\partial \phi}\bigg|_{\phi+2\pi} \tag{7c}$$

At the initiation of laser heating, the workpiece is in thermal equilibrium with the surroundings

$$T(r, \phi, z, 0) = T_\infty \tag{8}$$

4. Convection and radiation heat fluxes

Because it is possible that optimal LAM may be achieved by positioning the laser in such a way as to overlap the chamfer, the absorbed laser heat flux was determined by using a ninth order curvefit for the unmachined

$$\alpha_\ell q''_\ell = \alpha_\ell f(r/r_{\ell,p}) q''_{\ell,max} \tag{9a}$$

and the machined

$$\alpha_{\ell,m} q''_\ell = \alpha_{\ell,m} f(r/r_{\ell,p}) q''_{\ell,max} \tag{9b}$$

workpiece surfaces, where $q''_{\ell,max}$ and $f(r/r_{\ell,p})$ are prescribed by Rozzi [16] and $r_{\ell,p} = r_\ell/1.75$ is the radius of the beam cross-section containing 86.5% of the total laser power. The characteristic mode shape of the laser corresponds to a combination of TEM_{00} and TEM_{01} modes.

A gas assist jet is required in the laser assisted machining process to protect the CO_2 laser focusing optic from machining debris. The influence of workpiece motion on convection heat transfer in the impingement zone of the gas assist jet (Figs. 2 and 3) was neglected on the basis of the high jet exit velocity (>100 m/s) relative to the nominal workpiece surface speed (0.44 m/s) [7]. For an air mass flow rate of $\dot{m}_j = 2.08 \times 10^{-4}$ kg/s and a jet exit diameter and temperature of $D_j = 1$ mm and $T_j = 23°C$, the Reynolds number and dimensionless nozzle-to-surface distance were $Re_j = 14{,}400$ and $H_j/D_j = 10$, respectively. The jet center corresponds to the laser center (ϕ_c, z_c), and the extent of the jet interaction zone was determined by placing a few drops of ink on the surface of a stationary workpiece and measuring the pattern created by jet impingement. The spatial variation of the gas assist jet heat transfer coefficient was determined from existing experimental data [8,9], and heat transfer from the surface to the jet was then computed from the expression, $q''_{conv,j} = h_j[T(r_w, \phi, z) - T_j]$, where $T_j \approx T_\infty$. Mixed convection heat transfer coefficients on portions of the workpiece surface not exposed to the jet and on the free end and chamfer were determined from the empirical correlations of [10] and [11], respectively.

From reflectivity measurements made at $\lambda = 0.865$ μm on the opaque, sintered silicon nitride specimen of

interest in this study [12], the surface was found to be nearly diffuse and to have a reflectivity which is only weakly temperature dependent over the range from 23 to 1500°C. Assuming diffuse, temperature independent behavior to be characteristic of all wavelengths, existing data for the spectral distribution of the normal emissivity of sintered [13] and commercially available [14] silicon nitride indicate the near equivalence to the total emissivity of the unmachined surface and its absorptivity to radiation from the laser. Hence, it was assumed that $\varepsilon \approx \alpha_\ell \approx 0.83$. However, observations of the machined workpiece surfaces indicate a significant decrease in the intensity of the heated spot, and hence in the amount of thermal radiation absorbed at the wavelength corresponding to laser irradiation ($\lambda = 10.6$ μm). The machined workpiece surface therefore corresponds more closely to polished silicon nitride, for which measurements obtained from the literature [15] indicate a smaller value of the absorptivity to laser radiation ($\alpha_{\ell,\mathrm{m}} \approx 0.36$). The measurements also indicate retention of diffuse surface behavior and a total hemispherical emissivity of $\varepsilon_\mathrm{m} \approx 0.83$.

5. Thermal energy generation due to plastic deformation and tool–workpiece friction

For a machining process involving material removal by plastic deformation, volumetric heat generation in the primary shear zone may be expressed as

$$q'''_{\mathrm{pl}} = \frac{\varphi \dot{E}_\mathrm{s}}{\forall} \tag{10}$$

where φ is a known constant representing the fraction of the dissipated energy which is converted to sensible heat and $\forall$ is the volume of the primary shear zone. The rate of energy dissipation associated with material deformation may be expressed as $\dot{E}_\mathrm{s} = \int_\forall \dot{\varepsilon}\bar{\sigma}\mathrm{d}\forall$ where $\dot{\varepsilon}$ is the strain rate and $\bar{\sigma}$ the flow stress, which is assumed to be independent of the local strain. An approximate relation for the dependence of the flow stress on the strain rate and temperature does not exist for silicon nitride, nor is there a machining database from which such a relation could be developed.

In this study, $\dot{E}_\mathrm{s}$ was determined by using measured cutting forces with an energy balance for the machining process. Assuming no cutting tool flank or crater wear, the energy balance is of the form,

$$F_\mathrm{c}\bar{V}_\mathrm{w} = \dot{E}_\mathrm{s} + F_\mathrm{ct}V_\mathrm{chip} \tag{11}$$

where $\bar{V}_\mathrm{w}$ is the average workpiece velocity perpendicular to the cutting tool over the depth of cut,

$$\bar{V}_\mathrm{w} = \left(r_{\mathrm{w,\,m}} + \frac{d}{2}\right)\omega \tag{12}$$

and F_c is the main cutting force, which was experimentally measured [16]. The total cutting energy ($F_\mathrm{c}\bar{V}_\mathrm{w}$) is dissipated in material deformation ($\dot{E}_\mathrm{s}$) and friction along the tool rake face ($F_\mathrm{ct}V_\mathrm{chip}$). From three-dimensional machining measurements [16], the friction force, F_ct, and the average chip velocity, V_chip, on the tool rake face were determined, thereby enabling the calculation of $\dot{E}_\mathrm{s}$.

Since the tool feed is much less than the depth of cut ($L_\mathrm{f} \ll d$) for the operating conditions of this study, the influence of the shear plane angle on the workpiece temperature distribution may be neglected. Assuming the shear zone has a cross-sectional area identical to the material removal plane, the approximation of shear zone width proposed by Fenton and Oxley [17], $s_\mathrm{psz} \approx L_\mathrm{f}/10$, yields a primary shear zone volume of $\forall \approx dL_\mathrm{f}^2/10$. Adopting a value of $\varphi = 0.85$ from the literature [18,19], with the balance $(1-\varphi)$ representing strain energy stored within the chip, the following expression is then obtained for the heat generated per unit volume during plastic deformation,

$$q'''_{\mathrm{pl}} = \frac{0.85(F_\mathrm{c}\bar{V}_\mathrm{w} - F_\mathrm{ct}V_\mathrm{chip}}{(dL_\mathrm{f}^2/10)} \tag{13}$$

For a worn cutting tool, the total frictional energy generated at the tool flank may be expressed as $\dot{E}_\mathrm{flank} = \int_{A_\mathrm{flank}} \mu p V_\mathrm{w}\,\mathrm{d}A$, where μ is the coefficient of friction between the cutting tool and the workpiece, p is the local normal pressure on the tool perpendicular to the flank, and A_flank is the area associated with flank wear. However, since μ and p are not known for a silicon nitride workpiece and the cubic boron nitride cutting tool, the energy required to overcome friction at the tool flank and the area of flank wear were obtained experimentally [16].

A scaling analysis indicated that the portion of the thermal energy generated at the tool rake face by abrasion and by plastic deformation which is conducted into the workpiece is negligible compared to the thermal energy advected away from the workpiece with the heated chip. Hence, conduction of thermal energy from the chip to the workpiece due to heat generation at the tool rake face was neglected.

For a worn cutting tool, an additional term representing the rate of energy dissipation at the tool flank is required in the machining energy balance, which is now expressed as

$$(F_\mathrm{c}\bar{V}_\mathrm{w})_\mathrm{worn} = \dot{E}_\mathrm{s} + F_\mathrm{ct}V_\mathrm{chip} + \dot{E}_\mathrm{flank} \tag{14}$$

If Eq. (11), the cutting energy balance without tool wear, is subtracted from Eq. (14), for identical operating conditions, the rate of energy dissipation at the

tool flank may be found as,

$$\dot{E}_{\text{flank}} = (F_c \bar{V}_w)_{\text{worn}} - F_c \bar{V}_w \tag{15}$$

Assuming that heat dissipation at the tool flank interface is constant over the wear area, the resulting heat flux into the machined workpiece is then given by,

$$q''_{\text{flank}} = R_{\text{flank,w}} \frac{\dot{E}_{\text{flank}}}{A_{\text{flank}}} \tag{16}$$

where $R_{\text{flank,w}}$ is the fraction of energy generated at the workpiece–tool flank interface entering the workpiece. Substituting Eq. (15) into (16) and approximating the wear area as $A_{\text{flank}} \approx d\ VB_{\max}/2$ from experimental observations [16], the heat flux may be expressed as

$$q''_{\text{flank}} = \frac{R_{\text{flank,w}}\left[(F_c \bar{V}_w)_{\text{worn}} - F_c \bar{V}_w\right]}{\left(\dfrac{d\ VB_{\max}}{2}\right)} \tag{17}$$

where $VB_{\max}$ is the width of the flank wear scar. Although originally derived for the partitioning of thermal energy generation at the chip–tool interface, the analysis of Trigger and Chao [20] was used to specify $R_{\text{flank,w}}$, as

$$R_{\text{flank,w}} = \frac{\dfrac{8d(\dot{E}_{\text{flank}}/A_{\text{flank}})}{\pi k_t} - \overline{\Delta T}_w}{\dfrac{8d(\dot{E}_{\text{flank}}/A_{\text{flank}})}{\pi k_t} - \dfrac{4}{3\sqrt{\pi}} \dfrac{(\dot{E}_{\text{flank}}/A_{\text{flank}})}{k_w} \sqrt{\left(\dfrac{k_w}{\rho_w c_{p_w}}\right) \dfrac{[r_w - (d/2)]\phi_{\text{flank}}}{\bar{V}_w}}} \tag{18}$$

where $\overline{\Delta T}_w$ is the average temperature difference between the workpiece and the ambient at the cutting tool flank and $[r_w-(d/2)]\phi_{\text{flank}}$ is the average width of the flank wear region. Using high temperature properties of the silicon nitride ceramic workpiece and the cubic borin nitride cutting tool, a representative value for $\overline{\Delta T}_w$, and typical LAM operating conditions, a value of $R_{\text{flank,w}} \approx 0.9$ was determined and was held constant throughout the calculations.

6. Numerical procedure

The silicon nitride workpiece of interest is of 8.46 mm diameter and 57.2 mm length, with 5.53 mm long hemispherical ends. The radius and axial length of the computational domain were $r_w = 4.23$ mm and $L_{cv} = 38$ mm, respectively. For a machined length corresponding to $z_{\text{fe,o}}$ and a representative tool feed L_f of 0.01 mm, the spatial extent of control volumes in the z-direction was 0.33 mm for $0 \leqslant z < z_{\text{fe,o}}$, decreased linearly from 0.33 mm to 0.001 mm for $z_{\text{fe,o}} \leqslant z < [z_c + (D_\ell/2) - L_{\ell,a}]$, was held constant at 0.001 mm for $[z_c + (D_\ell/2) - L_{\ell,a}] \leqslant z < [z_c + (D_\ell/2) - L_{\ell,a} + L_f]$, and increased linearly thereafter to the end of the computational domain (L_{cv}). Such a discretization required 172 nodes. In the r- and ϕ-directions 32 and 52 nodes were employed, respectively. For the nominal operating condition, D_ℓ and $L_{\ell,a}$ are 2.5 and 0.38 mm, respectively, (ϕ_c, z_c) corresponds to (55 deg, 15 mm), and $z_{\text{fe,o}}$ and $z_c - z_{\text{fe,o}}$ are 11 and 0.42 mm, respectively.

The numerical scheme used to solve Eqs. (3)–(8) was identical to that used for laser heating without machining [6]. Temperature-dependent properties were used and updated at each iteration within a time step. During the preheat period, the laser center was located a distance $z_c - z_{\text{fe,o}}$ from the end of the workpiece to account for the thermal mass associated with the unmachined hemispherical section. Material removal (phase II) was initiated with the cutting tool located at a distance $L_{\ell,a}$ from the laser source. Computationally, this was accomplished by designating control volumes associated with the region $z_{\text{fe,o}} < z \leqslant z_c - L_{\ell,a}$ and $r_{w,m} < r \leqslant r_w$ as inactive at the time step immediately following the preheat phase. Because temperatures and temperature gradients in this region are small, this approximation had a negligible effect on the predicted temperatures.

The calculations were marched in time until the machined length corresponded to 11 mm. At each time step, a global energy balance convergence criterion was computed, which may be expressed as,

$$\left\{ P_\ell \Delta t - \left\{ \sum_1^N \rho \forall_n \Delta i_n + \left[q_{\text{conv}} + q_{\text{rad}} + (q_{\text{mr}} - q_{\text{pl}} - q_{\text{flank}}) \right] \Delta t \right\} \right\} / P_\ell \Delta t \leqslant 10^{-4}$$

where Δi_n and N are the enthalpy increase of control volume n during the time step and the total number of control volumes, respectively. This criterion had to be

satisfied for four consecutive iterations before proceeding to the next time step.

The entire temperature field at a given time step was considered converged if the energy balance was satisfied to less than 10^{-4} for four consecutive iterations. A grid sensitivity study was performed, with emphasis placed on the number of discrete steps and the number of axial control volumes per step required to achieve grid independence within the machining zone, which embodies a region of axial width L_f and radial depth d, extending about the cylinder circumference and within which axial control volumes are distributed uniformly. Ten axial control volumes, one per discrete step, were found to provide adequate spatial resolution of the temperature distribution in the machining zone. Control volume sizes in the r–ϕ plane were selected by achieving agreement between numerical predictions and a two-dimensional analytical solution for conduction in a rotating cylinder [21]. Decreasing the convergence criterion or increasing the overall grid density resulted in no significant change in the temperature field.

7. Experimental procedure

A laser assisted machining facility [6] consisting of a 1.5 kW CO_2 laser, a turret lathe, and a cutting tool equipped with a polycrystalline cubic boron nitride tipped carbide tool insert was utilized for the machining experiments. The laser power was controlled to within $\pm 4\% + 2$ W over the power range from 200 to 300 W, and the experimental uncertainty associated with determination of the beam diameter, D_ℓ, at the workpiece surface was ± 0.3 mm. The laser-tool lead distance, L_ℓ, was established to within ± 0.1 mm.

A fiber optic, single wavelength, laser pyrometer [12] was used to simultaneously measure the average spectral emissivity and temperature over a portion of the workpiece surface which measured 0.3 mm in diameter for temperatures exceeding 650°C. The circumferential distance between the translating CO_2 laser and the stationary laser pyrometer spot was established to within ± 0.1 deg and the distance from the pyrometer optic to the workpiece surface was fixed at 14 mm, which corresponds to calibration conditions for the laser pyrometer [12]. The experimental uncertainty of the surface temperature measurement ranged from $\pm 2.5\%$ at 1500°C to $\pm 15.5\%$ at 700°C [12].

The cutting tool position during the preheat phase was established according to the desired depth of cut, and the laser power and beam diameter were then set at the desired values. Prior to machining, low pressure (10 psi) laser assist gas (air) was forced into the cavity between the focusing optic and the laser exit location, protecting the optic from machining debris. Following activation of the data acquisition system, the CNC part program initiated workpiece rotation, and following the preheat phase traversed the laser and cutting tool with constant velocity, V_z, to the final position. Surface temperature and reflectivity measurements were made by the laser pyrometer at one of four lo-

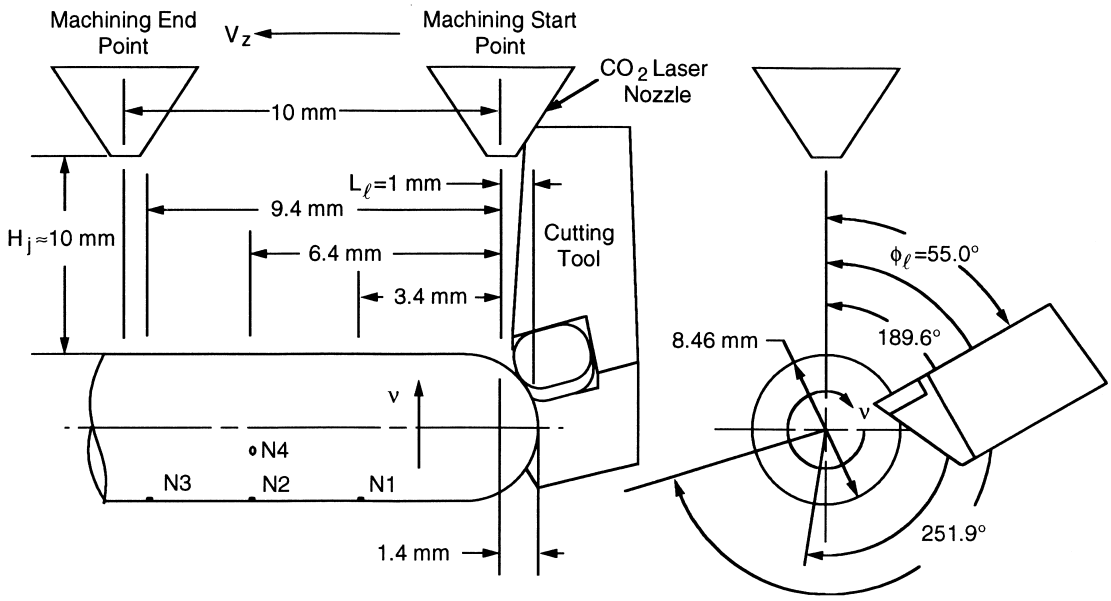

Fig. 4. Surface temperature measurement locations during laser assisted machining.

Table 1
Experimental operating conditions for the laser assisted machining of a silicon nitride workpiece

Case	v (rpm)	V_z (mm/min)	d (mm)	L_ℓ (mm)	D_ℓ (mm)	P_ℓ (W)
1	1000	10	1	1	2.5	250
2	500	10	1	1	2.5	250
3	2000	10	1	1	2.5	250
4	1000	20	1	1	2.5	250
5	1000	30	1	1	2.5	250
6	1000	10	1.5	1	2.5	250
7	1000	10	1	0.6	2.5	250
8	1000	10	1	2	2.5	250
9	1000	10	1	1	1.83	250
10	1000	10	1	1	3.84	250
11	1000	10	1	1	2.5	200
12	1000	10	1	1	2.5	300

cations on the silicon nitride workpiece (Fig. 4) as the laser and cutting tool traversed in the axial direction and the workpiece rotated relative to the pyrometer.

Experimental conditions of the study are given in Table 1. The depth of cut, d, was chosen to be large enough to minimize the influence of the cutting tool nose radius ($r_t = 0.625$ mm) and small enough to preserve the structural integrity of the workpiece. The ranges of laser translational velocity, V_z, beam power, P_ℓ, and diameter, D_ℓ, were selected to provide significantly different surface temperature distributions. The lower and upper bounds of P_ℓ were chosen to provide surface temperatures above 650°C, the minimum measurable by the laser pyrometer, and to avoid melting of the workpiece surface, respectively. The inverse was true for the prescribed values of V_z and D_ℓ. The range of the laser-tool lead distance, L_ℓ, permitted examination of the effect of laser radiation deposited on the unmachined workpiece surface, which increases with increasing L_ℓ. For $D_\ell/2 > L_\ell$, the laser beam will overlap the chamfer. The preheat time, t_p, was fixed at ten seconds. All of the experiments involved removal of one layer of material, at a constant depth of cut d and over a machined length of 10 mm, from a sintered silicon nitride workpiece of diameter 8.46 mm and length 57.2 mm, with 5.53 mm long hemispherical ends.

Several experiments performed at nominal operating conditions (Case 1 of Table 1) enabled calculation of cutting forces corresponding to zero tool flank wear [16]. The corresponding value of q'''_{pl} obtained from Eq. (13) was found to be 1.1×10^{15} W/m^3. Additional experiments performed for the nominal conditions involved flank wear, and a value of $\phi_{flank} \approx 0.06$ deg was determined for the circumferential extent of the wear region. From Eq. (17), a value of $q''_{flank} \approx 9.45 \times 10^7$ W/m^2 was determined for the heat flux at the workpiece–tool flank interface. For the nominal condition, the prescribed values of q'''_{flank} and q''_{flank} correspond to values of q_{pl} and q_{flank} of 11 and 4 W, respectively. Computation of q_{pl} and q_{flank} values from the experimental data [16] for other operating conditions revealed that the values of q_{pl} and q_{flank} calculated at the nominal operating condition were representative of all LAM operating conditions. The values of q_{pl} and q_{flank} calculated at the nominal operating condition were therefore held constant for this study.

8. Comparison of experimental and numerical temperature histories

The computed surface temperatures represent an area weighted average of the workpiece control volumes beneath the 0.3 mm diameter pyrometer spot. The moment the stationary pyrometer spot acquired radiant energy emitted by the chamfer interface or machined surface, the effective distance between the pyrometer and the measurement surface changed from the required value of 14 mm and data acquisition was terminated. However, the numerical simulation was allowed to continue well beyond this point in time.

Fig. 5 illustrates measured and predicted temperature histories at three axial locations (N1, N2, and N3) for nominal operating conditions (Case 1 of Table 1). Workpiece conduction in the axial direction transports thermal energy to each measurement location during the preheat phase, and as the laser approaches. The temperature reaches a peak value as the laser spot passes the r–ϕ plane of the measurement location, and subsequently decays, largely due to radial and axial conduction of energy from the heated surface. The first computational result after the peak temperature represents an average of control volumes on the machined and unmachined surfaces, after which average temperatures represent those of the machined surface. After the laser and cutting tool have passed a particular measurement location, the temperature decreases due to radial and axial conduction, as well as surface convection and radiation losses. While the model may have slightly underpredicted the surface temperature on the unmachined workpiece surface as the laser approaches for the nominal operating conditions at measurement station N2, the agreement between the measurements and predictions is, in general, excellent with the majority of the data falling within $\pm 5\%$ of the predictions.

As the workpiece rotates away from the laser source, thermal energy is transported from the surface by the three modes of heat transfer, and circumferential surface temperature gradients decrease with increasing dis-

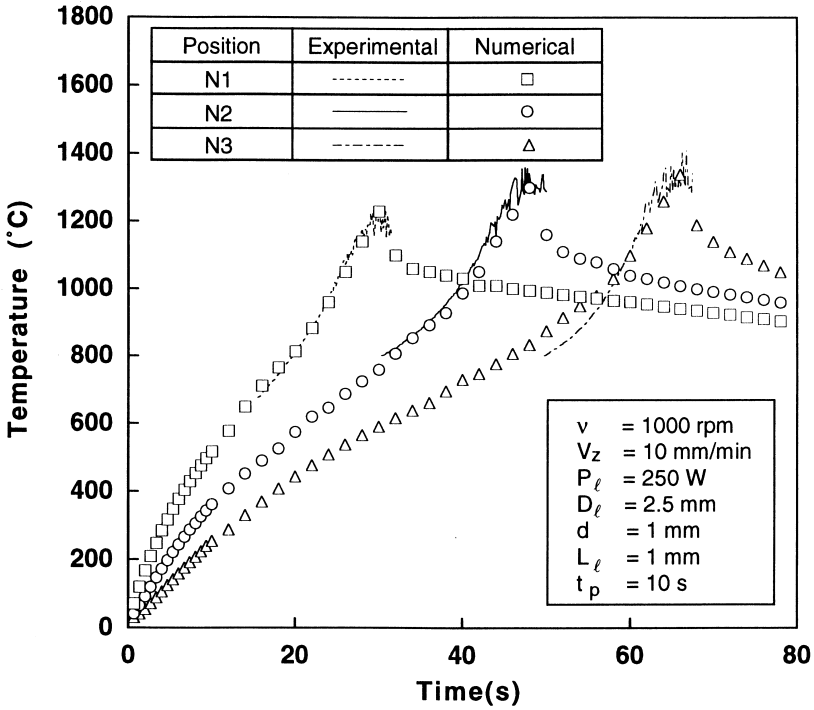

Fig. 5. Experimental and numerical surface temperature histories for nominal operating conditions at selected axial positions (N1, N2, and N3).

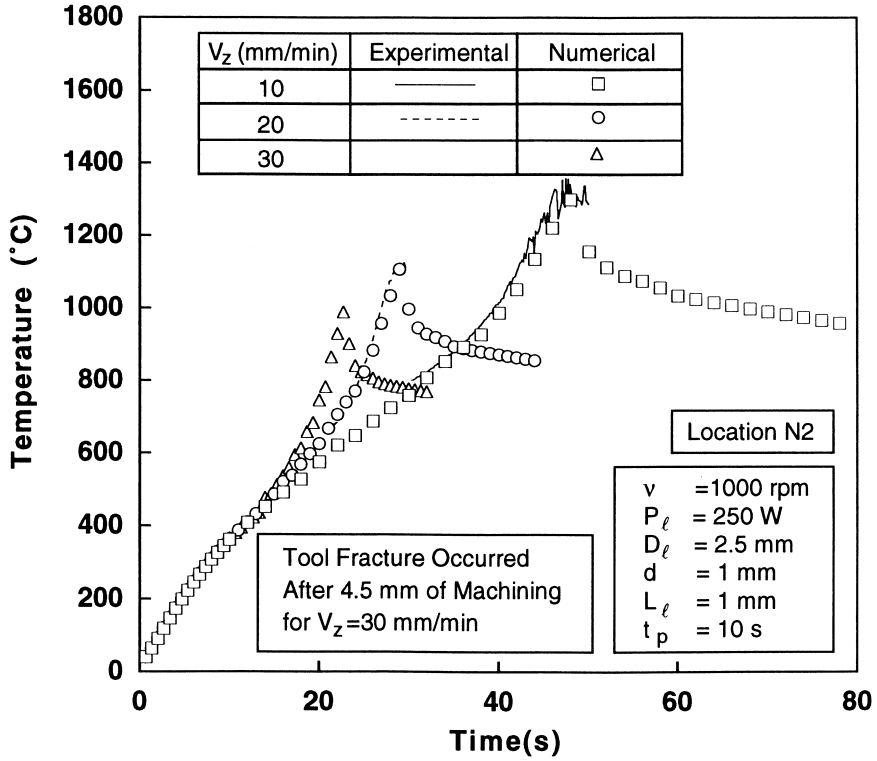

Fig. 6. Effect of laser/tool translational velocity on experimental and numerical surface temperature histories at location N2.

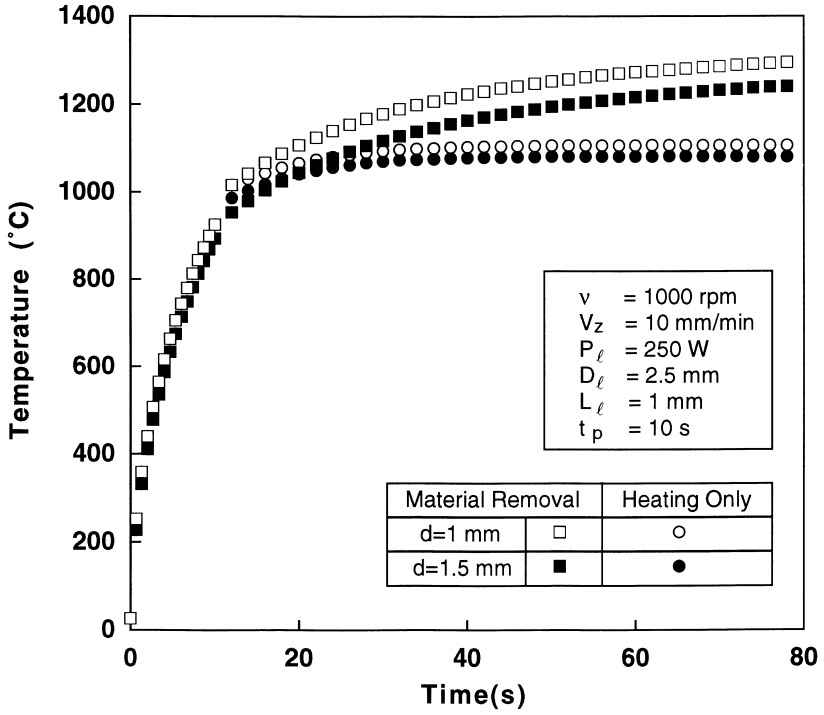

Fig. 7. Comparison of the average temperature at the material removal plane for $d = 1$ and 1.5 mm and the average temperature of a comparable region for a simulation without material removal.

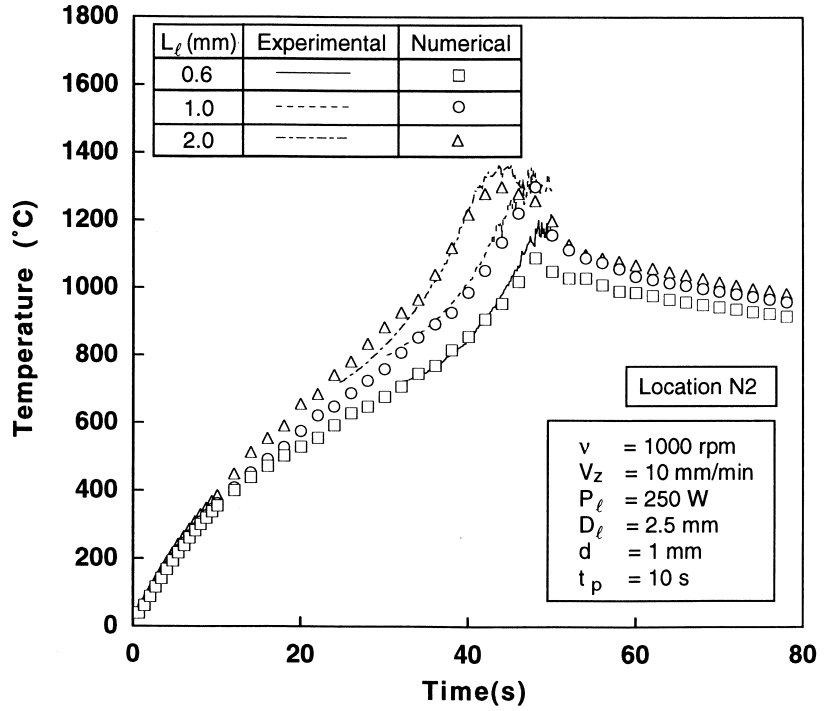

Fig. 8. Effect of laser-tool lead distance on experimental and numerical surface temperature histories at location N2.

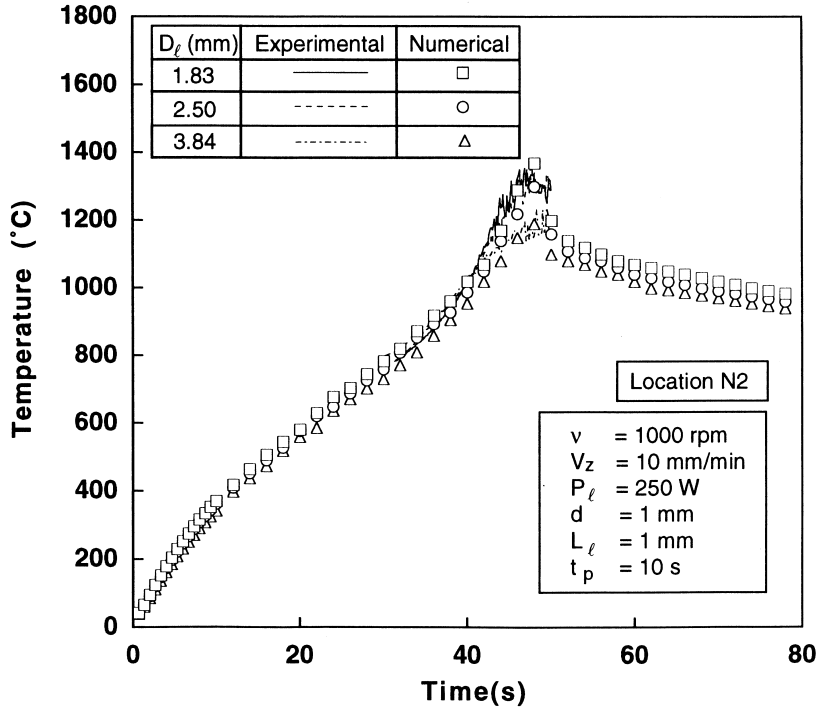

Fig. 9. Effect of laser diameter on experimental and numerical surface temperature histories at location N2.

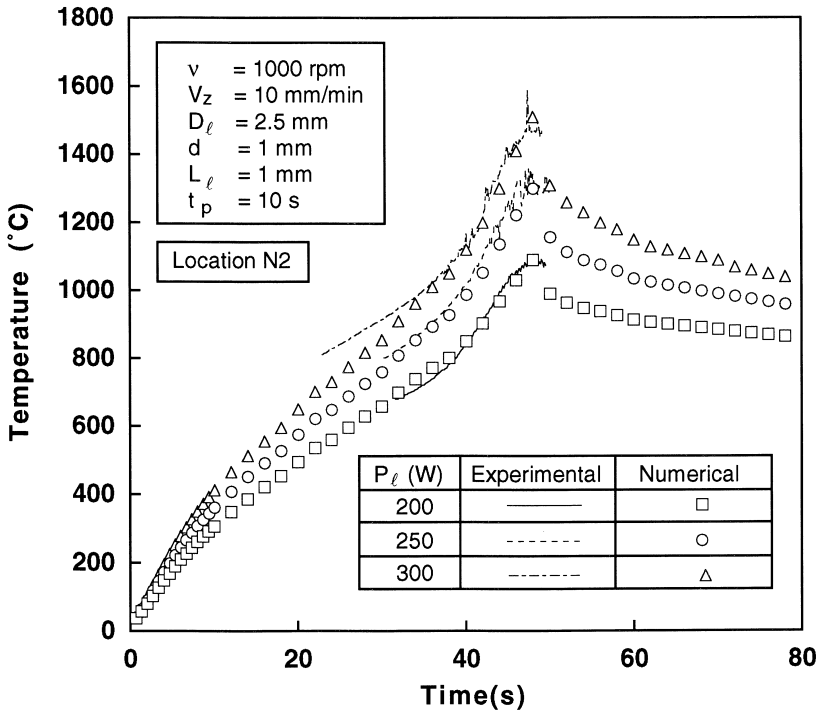

Fig. 10. Effect of laser power on experimental and numerical surface temperature histories at location N2.

tance from the laser source. As circumferential advection increases with increasing workpiece rotational speed, v, the peak value of the surface temperature at location N2 increases.

The amount of laser energy deposition decreases with increasing laser/tool translational velocity, V_z, causing the surface temperatures to decrease, as illustrated in Fig. 6. For the highest laser/tool translational velocity, $V_z = 30$ mm/min, cutting tool fracture occurred after a machined length of 4.5 mm. At this location the near-chamfer surface temperature, $T_{s,ch}$, which is defined as the arithmetic average of the last two measurements at a particular pyrometer location before the chamfer entered the pyrometer viewing area, was approximately 980°C, and the temperature at a radial location corresponding to the depth of cut may have been below or near the lower bound of the transition temperature range for YSiAlON glass, which is from 920 to 970°C [22]. A value of $T_{s,ch}$ below this range would significantly increase the material strength and brittleness and consequently the propensity for tool fracture.

The relatively low heat transfer rates associated with mixed convection and emission from the chamfer surface to the ambient air and surroundings, respectively, render the chamfer a significant thermal resistance to heat transfer in the z-direction compared to the corresponding conduction resistance for similar operating conditions without material removal. This behavior is clearly illustrated in Fig. 7, which compares the temperature averaged over the material removal plane for $d = 1$ and 1.5 mm with the average temperature over an identical region computed from a simulation without material removal. The increase of the depth of cut for machining increases the rate of material removal for a fixed workpiece rotational speed and, correspondingly, decreases the average (Fig. 7) and the maximum temperatures over the material removal plane due to the increased thermal energy leaving the workpiece. However, the influence of an increasing depth of cut is insignificant at measurement location N2 due to conduction within the workpiece.

Since the amount of energy deposition within the unmachined portion of the workpiece increases with increasing laser-tool lead distance, L_ℓ, there is a corresponding increase in the temperature of the unmachined workpiece surface as illustrated by Fig. 8. As L_ℓ increases, the time required for the laser center location to pass the stationary pyrometer for the same machined length decreases because the initial cutting tool location was identical for each experiment. Hence, the peak temperature occurs sooner for increasing L_ℓ. After the peak, the temperature histories begin to converge due to the strong influence of conduction heat transfer on the surface temperature distribution.

As shown in Figs. 9 and 10, surface temperatures increase with decreasing laser beam diameter and increasing laser power which correspond to an increase in the maximum laser heat flux and energy deposition, respectively.

Numerical simulations have been performed to assess the sensitivity of the predicted temperatures to uncertainties in the thermophysical and radiative properties. Temperatures in proximity to the material removal zone decrease with increasing k, c_p, and ε, and if each property is independently varied by $\pm 20\%$, the maximum ranges of the corresponding temperature variations are approximately ± 60°C, ± 80°C and ± 50°C, respectively. These variations occur during intermediate stages of the LAM process, but decrease as quasi-steady conditions are approached. Temperatures increase with increasing α_ℓ, and for a $\pm 20\%$ uncertainty, variations as large as ± 200°C are associated with intermediate stages of the process. Temperatures decrease with increasing values of the convection coefficient associated with the gas assist jet and vary by as much as ± 25°C for a $\pm 10\%$ variation in h_j.

9. Conclusions

A three-dimensional thermal model has been developed for a laser assisted machining process, and the model has been validated by comparing predicted surface temperature histories with measurements made using a focused laser pyrometer. For a turning operation involving a silicon nitride workpiece, predictions and measurements were made to determine the effect of the workpiece rotational and laser/tool translational speeds, depth of cut, laser-tool lead distance, and the laser beam diameter and power, on surface temperatures at prescribed circumferential and axial locations.

For the laser-tool traverse distance of this study, the experiments and the predictions revealed that near-laser, quasi-steady conditions are not achieved, thereby requiring characterization of the process as time-dependent. The peak temperature at the measurement location increases slightly with increasing rotational speed due to the effect of increasing circumferential advection. The amount of energy deposition within the unmachined workpiece decreases with decreasing laser power, decreasing laser-tool lead distance and/or increasing laser/tool translational velocity, thereby reducing the temperature along the machined chamfer surface. If this temperature is less than the lower bound of the YSiAlON glass transition temperature range, tool fracture may occur. The maximum laser heat flux and, consequently, the maximum surface temperature decreases with increasing beam diameter. While decreasing the average and maximum temperatures over the material removal plane, an increasing

depth of cut does not significantly influence the surface temperature distribution at a location which is circumferentially removed from the cutting tool.

Acknowledgements

The authors gratefully acknowledge the support of the National Science Foundation through Award Number 9400654-CTS and Mr. Tom Yonushonis and Mr. Bill Mandler of Cummins Engine Co. and Enceratec, respectively, for their interest in the project and their donation of the silicon nitride samples used in the experiments.

References

[1] J.C. Rozzi, F.P. Incropera, Y.C. Shin, Transient, three-dimensional heat transfer model for the laser assisted machining of silicon nitride: II. Assessment of parametric effects, International Journal of Heat and Mass Transfer 43 (2000) 1425–1437.

[2] W. König, A.K. Zaboklicki, NIST Special Publication 847, National Institute of Science and Technology, 1993.

[3] K. Uehara, H. Takeshita, Cutting ceramics with a technique of hot machining, Annals of the CIRP 35 (1) (1986) 55–58.

[4] T. Kitagawa, K. Maekawa, Plasma hot machining for new engineering materials, Wear 139 (1990) 251–267.

[5] W. König, A. Wageman, Fine Machining of Advanced Ceramics, in: P. Vincenzini (Ed.), Ceramics Today — Tomorrow's Ceramics, Montecatini Terme, Italy, 1991, pp. 2769–2784.

[6] J.C. Rozzi, F.E. Pfefferkorn, F.P. Incropera, Y.C. Shin, Transient thermal response of a rotating cylindrical silicon nitride workpiece subjected to a translating laser heat source: I — comparison of surface temperature measurements with theoretical results, ASME Journal of Heat Transfer 120 (4) (1998) 899–906.

[7] D.A. Zumbrunnen, Convective heat and mass transfer in the stagnation region of a laminar planar jet impinging on a moving surface, ASME Journal of Heat Transfer 113 (1991) 563–570.

[8] M.S. El-Genk, L. Huang, Z. Guo, Heat transfer between a square flat plate and a perpendicularly impinging circular air jet, in: M.B. Pate and M.K. Jensen (Eds.), Proceedings of the 28th National Heat Transfer Conference and Exhibition, vol. HTD-202, Enhanced Heat Transfer, San Diego, CA, 1992, pp. 33–38.

[9] R.J. Goldstein, A.I. Behbahani, K.K. Heppelmann, Streamwise distribution of the recovery factor and the local heat transfer coefficient to an impinging circular gas jet, International Journal of Heat and Mass Transfer 29 (8) (1986) 1227–1235.

[10] G.A. Etemad, Free-convection heat transfer from a rotating horizontal cylinder to ambient air with interferometric study of flow, ASME Journal of Heat Transfer 77 (1955) 1283–1289.

[11] P.D. Richardson, O.A. Saunders, Studies of flow and heat transfer associated with a rotating disc, Journal of Mechanical Engineering Science 5 (4) (1963) 336–342.

[12] F.E. Pfefferkorn, J.C. Rozzi, F.P. Incropera, Y.C. Shin, Surface temperature measurement in laser assisted machining processes, Experimental Heat Transfer 10 (4) (1997) 291–313.

[13] Y.S. Touloukian, Thermophysical Properties of High Temperature Solid Materials, Macmillan, Purdue University, 1967.

[14] D.P. DeWitt, G.D. Nutter, Theory and Practice of Radiation Thermometry, Wiley, New York, 1988.

[15] T. Makino, T. Kunitomo, I. Sakai, H. Kinoshita, Thermal radiation properties of ceramic materials, Transactions of the Japan Society of Mechanical Engineers 50 (452) (1984) 1045–1052.

[16] J.C. Rozzi. Experimental and theoretical evaluation of the laser assisted machining of silicon nitride. PhD thesis, Purdue University, 1997.

[17] R.G. Fenton, P.L.B. Oxley, Mechanics of orthogonal machining: predicting chip geometry and cutting forces from work-material properties and cutting conditions, Proceedings of the Institution of Mechanical Engineers 184 (49) (1969–70) 927–942.

[18] G.I. Taylor, H. Quinney, The latent energy remaining in a metal after cold working, Proceedings of the Royal Society of London: Series A 143 (1934) 307–326.

[19] G.I. Taylor, H. Quinney, The emission of latent energy due to previous cold working when a metal is heated, Proceedings of the Royal Society of London: Series A 163 (1937) 157–181.

[20] K.J. Trigger, B.T. Chao, An analytical evaluation of metal cutting temperatures, Transactions of the American Society of Mechanical Engineers 73 (1951) 57–68.

[21] B. Gecim, W.O. Winer, Steady temperature in a rotating cylinder subject to surface heating and convective cooling, ASME Journal of Heat Transfer 106 (1984) 120–127.

[22] S. Hampshire, R.A.L. Drew, K.H. Jack, Viscosities, glass transition temperatures, and microhardness of Y-Si-Al-O-N glasses, Journal of the American Ceramic Society 76(3) (1984) C-46–C-47.